Transport in Porous Media 5: 247–268, 1990.

Wetting Front Instability in Unsaturated Porous Media: A Three-Dimensional Study in Initially Dry Sand

ROBERT J. GLASS
Geoscience Analysis Division 6315, Sandia National Laboratories, Albuquerque, NM 87185, U.S.A.

STEVE CANN, JEFF KING, NATHAN BAILY, J-YVES PARLANGE, and TAMMO S. STEENHUIS
Department of Agricultural and Biological Engineering, Cornell University, Ithaca, NY 14853, U.S.A.

(Received: 7 September 1989; revised: 21 November 1989)

Abstract. Three-dimensional fingers caused by gravity driven, wetting front instability in unsaturated porous media were explored through laboratory experimentation. Two sets of experiments were conducted using initially dry sand in large 30 cm diameter columns to guide analytical development for finger velocity and diameter. The first set consisted of ponding water on a two-layer sand system with a fine sand overlying a coarse sand. Here, a complicated pattern of interaction among fingers was found to occur. In the second set, water was applied directly to the coarse layer as 2 cm diameter area sources, enabling systematic study of individual finger structure. Based on dimensional analysis and the experimental results, general relationships were found for finger velocity and cross-sectional area as a function of both the flux through the finger and hydraulic properties of the coarse layer represented by the sorptivity, saturated conductivity, and initial and saturated moisture contents. Unlike the two-dimensional case, air entrapment was an important factor in explaining the experimental results.

Key words. Unsaturated flow, instability.

1. Introduction

The subsurface transport of water and contaminants through the unsaturated and saturated zones has been found to be extremely variable in time and space. To explain the spatial and temporal distribution of solutes in these zones, much emphasis has been placed on spatial variability in hydraulic properties and in 'macropore flow' through cracks, animal burrows, or root holes. However, another factor contributing to transport variability may be flow instability.

A wide variety of instabilities and fingering patterns may occur in porous media. Most often the instabilities are driven by either viscous or gravity forces, or both. In viscosity-driven instability (for a recent review, see Homsy, 1987), the displacement of one fluid by another of different viscosity is found to be unstable when the less viscous fluid displaces the more viscous fluid at a sufficiently high displacement flow rate. When this instability occurs (often termed viscous fingering) fingers form, causing the bypass of a large volume of the porous medium. If the two fluids are immiscible, surface tension between the fluids within individual pores is found to have a stabilizing influence when the medium is wettable to the

invading fluid. For miscible fluids, diffusion and hydrodynamic dispersion at the front play a stabilizing role. Stabilization by these mechanisms restricts the range of wavelengths that are unstable and thus influences stability criteria.

In hydrology, where gravity is often the major driving force, gravity-driven instability has many examples. Any time a more dense fluid overlies a less dense fluid, an instability may result through which the fluids are overturned. Examples are ubiquitous including heavy contaminants such as halogenated organic solvents released above the water table and salt water layered upon fresh water. Again, as in viscosity-driven instabilities, the instability is restricted to wavelengths above a lower threshold by capillarity and diffusion/dispersion processes operating at the fluid-fluid interface for immiscible and miscible fluids, respectively. It is interesting to note that diffusion itself may play a destabilizing role when more than one component that affects fluid density is present in a system (Green, 1984; Turner, 1985). There, if two or more components diffuse at different rates, gravity-driven instabilities in multi-component systems may occur. Such 'multi-component convection' processes may be important in understanding fluid and contaminant transport and mixing processes in multi-contaminant systems.

A simple situation where gravity-driven instability can cause fingers to form is the downward infiltration of liquid into a gas-filled, or unsaturated, homogeneous porous medium. The linear stability analysis of Saffman and Taylor (1958) suggests that the liquid-gas interface will be unstable if its velocity is less than the saturated liquid velocity of the medium. The inclusion of capillary effects at the interface restricts unstable wavelengths to be above a minimum threshold dependent on the properties of the medium (Chouke *et al.*, 1959; Parlange and Hill, 1976). From the point of view of hydrology where horizontal length scales are not restricted, potentially unstable circumstances commonly occur and the instability has been termed 'wetting front instability'.

Wetting front instability has been observed experimentally in both the laboratory (e.g., Tabuchi, 1961; Miller and Gardner, 1962; Peck, 1965; Smith, 1967; Hill and Parlange, 1972; White *et al*, 1976; Glass and Steenhuis, 1984; Diment and Watson, 1985; and Tamai *et al.*, 1987) and in the field (e.g., Starr *et al.*, 1978; Starr *et al.*, 1986; Glass *et al.*, 1988; van Ommen *et al.*, 1988; Hendrickx *et al.*, 1988, and van Ommen and Dijksma, 1988). Most recently it has been studied experimentally in thin slab chambers (1 cm or approximately 10 mean grain sizes in thickness) that force macroscopic two-dimensional flow in initially dry porous media (Glass *et al.*, 1989b,c). The development of new techniques for visualization of the moisture content within such thin slab chambers has allowed understanding of the basic mechanism of finger persistence (Glass *et al.*, 1989c). While results in two dimensions are important for checking theory and in advancing the understanding of the phenomenon, exploration of wetting front instability in three-dimensional systems is crucial for obtaining results applicable in the field. A three-dimensional study poses experimental difficulties above those in two dimensions. Because fingers in large diameter columns form within the porous medium and cannot be seen from the sides of a chamber, the measurement of finger velocities and cross-sectional areas or diameters is much more difficult than in two-dimensional experiments.

This paper presents the results of experimental studies that explore wetting front instability in large-diameter columns where full three-dimensional behavior occurs. Two sets of experiments are carried out. In the first set, the effect of the flow rate through the system on unstable flow field behavior in initially dry sand is explored. Flow rate is varied through the texture of the top, lower conductivity, layer. In a second set of experiments, individual fingers are simulated directly from area sources to determine accurately relationships between the finger properties, porous media properties, and the flow rate through individual fingers in initially dry sand.

2. Theory

Unstable flow field behavior as defined by finger width (or diameter in our case) and finger velocity may be related through dimensional analysis to relevant system parameters (Glass *et al.*, 1989a). Finger diameter, d, in an isotropic and homogeneous porous medium is shown to be a function of the layer properties, the initial moisture content, θ_i, and the top boundary condition given as the average flux entering the individual finger from above, q_F. The value of q_F is given by the flow rate through an individual finger, Q_F, divided by the cross-sectional area of the finger, A. The layer properties selected through a nondimensionalization of the Richards' Equation are the saturated conductivity, K_s, and the square of the sorptivity, S^2, where S is evaluated between θ_i and the saturated value of the moisture content, θ_s, corresponding to a potential of ψ_{ae}, the water entry value. The ratio of K_s and S^2 divided by $(\theta_s - \theta_i)$, yields a length scale that embodies the ratio of capillary to gravity forces and thus is a relevant scaling factor for the finger diameter. Therefore a dimensionless parameter, the gravity-capillarity ratio, N, is defined as

$$\mathbf{N} = \frac{\mathrm{d}K_s(\theta_s - \theta_i)}{S^2}. \tag{1}$$

The average flux through the finger, q_F, divided by K_s of the layer yields a second dimensionless parameter, $\mathbf{R}_F$, termed the flux-conductivity ratio

$$\mathbf{R}_F = \frac{q_F}{K_s} \tag{2}$$

which should also influence finger width. Through dimensional analysis it may be shown that N must be a function of $\mathbf{R}_F$ and so d is found to be

$$d = \frac{S^2}{(\theta_s - \theta_i)K_s} f_{dF}(\mathbf{R}_F) \tag{3}$$

where f_{dF} is a function of $\mathbf{R}_F$ not yielded by dimensional analysis.

To obtain a similar relationship for the finger velocity, v, a third dimensionless parameter, the velocity-conductivity ratio, $\mathbf{R}_{vF}$, is defined

$$\mathbf{R}_{vF} = \frac{v(\theta_s - \theta_i)}{K_s} \tag{4}$$

and because N and $\mathbf{R}_F$ are related by Equation (3), dimensional analysis shows $\mathbf{R}_{vF}$ to be a function of $\mathbf{R}_F$ as well

$$v = \frac{K_s}{(\theta_s - \theta_i)} f_{vF}(\mathbf{R}_F) \tag{5}$$

where f_{vF} is a function of $\mathbf{R}_F$, again not given by dimensional analysis.

Equations (3) and (5) are general and are not dependent on the dimensionality of the fingers. The functions $f_{dF}(\mathbf{R}_F)$ and $f_{vF}(\mathbf{R}_F)$, however, may have different forms in two or three dimensions where d in two dimensions would correspond to the width of a finger while in three dimensions d would correspond to the diameter of a cylindrical finger. The functions $f_{dF}(\mathbf{R}_F)$ and $f_{vF}(\mathbf{R}_F)$ may be found through either analytical or experimental approaches. Analytical approaches to determine these functions are founded on linear stability theory and thus approximate reality (e.g., Philip, 1975; and Parlange and Hill, 1976 for the two-dimensional case). Because it is often difficult to choose the proper approximation when a phenomenon has not been adequately described experimentally, the experimental approach is important for guiding analytical development. Such a combination was used for the two-dimensional case to show correspondence between analytical and experimental results for $f_{dF}(\mathbf{R}_F)$ (Glass *et al.*, 1989b).

The stability of a given three-dimensional, vertical infiltration system depends on the expected finger diameter calculated for the layer and the maximum horizontal dimension of the system. If the finger diameter is less than the maximum horizontal system dimension, then instability is expected; otherwise the system is stable. So, for N calculated with L_s, the maximum horizontal system width, substituted for d, Equation (3) yields

$$\mathbf{N} < f_{dF}(\mathbf{R}_F) \tag{6}$$

for stability. The application of (6), however, is difficult as it is the flux through the system that is usually known and not the flux through individual fingers. In very homogeneous systems, Glass *et al.* (1989b) found that for the two-dimensional case, fingers that form with a given flux through the system, q_S, will have very similar flow rates and cross-sectional areas; thus, the average flux through a finger, $\overline{q_F}$, and q_S may be related by

$$\overline{q_F} = \beta q_S \tag{7}$$

β is defined by $A_S/n\overline{A_F}$ where n is the number of fingers, A_S is the average finger cross-sectional area, and A_S is the cross-sectional area of the system. β is simply the reciprocal of the fractional cross-sectional area of the chamber in fingers and

will itself be a function of $\overline{q_F}$ that must be found experimentally. For homogeneous systems, (6) may be applied after β has been determined. In more heterogeneous systems, where all fingers may eventually merge into one, (6) may be better applied with Q_s substituted for Q_F.

Thus N, $\mathbf{R}_F$, and $\mathbf{R}_{vF}$ parameterize both stability and finger properties through the relations in Equations (3), (5), and (6). All three of these dimensionless parameters will be influenced by initial moisture content through its effect on porous media properties K_s and S^2 as well as the initial condition $(\theta_s - \theta_i)$. Using the concept of similarity developed by Miller and Miller (1956), N, $\mathbf{R}_F$, and $\mathbf{R}_{vF}$ may also be scaled to yield the effects of mean grain size and fluid properties (Glass *et al.*, 1989a). Models that relate mean grain size, grain size distribution, and bulk density to hydraulic properties (e.g. Haverkamp and Parlange, 1986) can be used to demonstrate the effects of these on stability and finger properties as well.

It is also important to note that $\mathbf{R}_F$ and $\mathbf{R}_{vF}$ simply scale the flux through the finger and finger velocity by the maximum value of each that may be attained for a specific system under unit hydraulic head gradient. In Glass *et al.* (1989a,b) these values were taken as K_s and $K_s/(\theta_s - \theta_i)$ respectively, yielding Equations (2) and (4). However, because of other complicating effects such as air entrapment, these values may be different and $\mathbf{R}_F$ and $\mathbf{R}_{vF}$ redefined accordingly.

3. Experimental Method

The special experimental methods and procedures developed for the study of wetting front instability in two-dimensional slab chambers by Glass *et al.* (1989b) were adapted for three-dimensional systems in the present study.

3.1. EXPERIMENTAL SANDS

The sands used in the experiments were generated from commercially available white silica sand by mechanical sieving. The coarse bottom layer, in which fingers were studied, was composed of 14 to 20 fraction sand (U.S. sieve series, 1.25 mm to 0.7 mm). Finer top layers are also referred to by the sieves that define their fraction. The sand was cleaned before and between uses with hot soapy water after which it was rinsed thoroughly with tap water followed by distilled water. The sand was dried in an oven at 50°C and, because no effort was made to restrict movement of water vapor from the air into the sand after drying, the initial moisture content, while not zero, was very close to zero. The grain size distribution of the 14–20 sand used in these experiments was skewed toward the fine end compared to the same 14–20 sand used in the two-dimensional study (Glass *et al.*, 1989b) and thus measured K_s and S were lower.

3.2. EXPERIMENTAL CHAMBER, FILLING AND PACKING

The chamber consisted of twelve 30 cm diameter rings 5 cm in height. The rings were held between two 38 cm square aluminum end plates by four sets of cables equipped with turnbuckles attached to each of the plates which were tightened to hold the rings in place (Figure 1a). Four thin aluminum shims were placed between the rings at each level in line with the four holding cables before tightening. These were to create small cracks between the rings so that air could escape freely and water movement would not be affected by any internal air pressure buildup in the chamber. The top plate had a 30 cm diameter hole corresponding to the chamber diameter.

The chamber was filled through an extension consisting of three 30 cm diameter rings (Figure 1b). The top, middle, and bottom rings were 20, 30, and 10 cm high, respectively. Between the top and middle rings, a piece of perforated sheet metal with approximately 4 mm holes was placed to reduce the sand fill rate. Between the middle and bottom rings and the top plate, two fine (4 mm) wire screens were placed to further randomize the falling sand. The filling apparatus was inserted on top of the chamber and sand was poured into the top, maintaining the level of sand in the filling extension higher than the perforated screen so that an even distribution of sand was ensured.

When filled with sand, the chamber was packed with a drop impact method using a packing apparatus that lifted the chamber 1.25 cm and then dropped it to the ground. After packing, the upper 30 cm of sand was removed as it was found

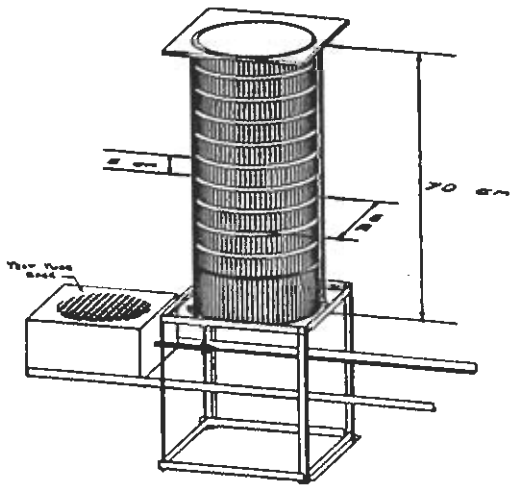

Fig. 1a. Drawing of experimental chamber.

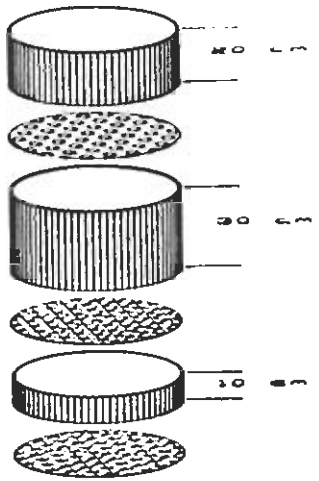

Fig. 1b. Drawing of chamber filling extension.

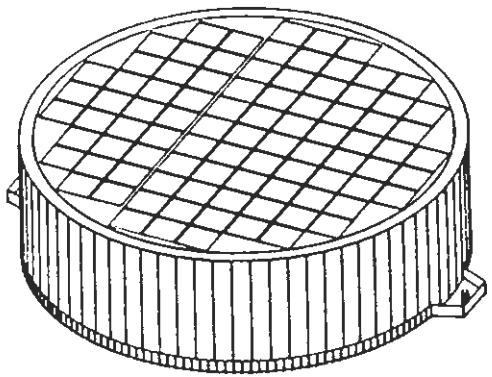

Fig. 1c. Drawing of chamber drip section flow distribution sampler.

to be of a lower bulk density than below, where the bulk density was a constant reproducible 1.59 g/cm^3. For the two-layer experiments, a thin piece of paper towel was placed on top of the bottom layer to ensure a sharp textural interface, and the top layer was added and packed using the traditional tamping method.

3.3. DATA MEASUREMENT

To measure the cross-sectional area of fingers that formed in a particular experiment, we relied on the fact that for coarse sands, the time scale for vertical finger growth is much less than the time scale for horizontal finger widening. When an experiment is sufficiently brief, measurement of finger cross-sectional areas by disruptive sampling after the experiment leads only to slight overestimation of finger dimensions. So that the wet regions could be easily seen, distilled water with a low concentration of USDA Red #3 (0.025%) was used in the experiments. The column was cut up rapidly after an experiment to expose finger cross-sections with depth, the surface was cleaned with a vacuum to remove sand that had been moved during the slicing process, and finger cross-sectional areas were drawn on acetate sheets. The areas of the individual fingers were then measured from the drawings.

All experiments were conducted at a constant 20°C within a controlled environmental chamber. The flow rate through individual fingers was monitored through a 'drip section' that constituted the lowest section in the chamber. The drip section was constructed out of an array of 10 cm high, 2.5 cm square tubes brazed together into a checkerboard pattern. The tube array was installed on a slab of PVC that formed the bottom of the chamber around which was glued a 10 cm high ring of the chamber PVC pipe. At the bottom of each tube a brass nozzle containing a wire screen was installed. The height of the tubes, 10 cm in this case, was higher than the capillary fringe of the sand in the chamber so that sideways movement within the saturated zone that forms at the bottom of the chamber was restricted and the flow entering the tube at the top could be measured. The drip section allowed the monitoring of the flow distribution and its evolution in time through the 97 ports (Figure 1c).

Finger tip velocity was measured electrically by using the finger as a switch. An electrical potential was placed between the fluid at the top of the chamber and the individual screens at the bottom of each drip section. The potential drop across resistors connected to each of the 97 screens at the bottom was monitored for all of the screens once a second using an analogue-to-digital converter and recorded on an IBM AT. When a finger tip arrived at the bottom of one of the drip sections, the voltage would jump as the circuit was completed.

3.4. EXPERIMENTS CONDUCTED

Two types of experiments were conducted to determine finger velocity and diameter in initially dry sand as functions of the dimensionless flux-conductivity ratio, $\mathbf{R}_f$. The first type were ponded, two-layer experiments with a fine-textured layer overlying the coarse 14–20 sand. A series of four two-layer experiments was conducted using three different top layers (see Table I) at a ponding level of 1.5 cm above the top sand layer. Only fingers that were isolated from the other fingers could be used to determine relationships between Q_f, $\mathbf{R}_f$, d, and v. Because of

Table I. Three-dimensional two-layer experiments

Exp. number	Top layer (Sieve #)	Fraction of chamber occupied by fingers	Q_f (ml/min)	Number of fingers	Average finger area (cm²)	Average finger velocity (cm/min)
1	140–200	0.49	*	36	9.9	*
2	140–200	0.36	329.4	30	8.5	*
3	40–50	0.83	3201	**	**	45–50
4	100–140	0.32	349.4	36	6.3	15

* was not measured.
** could not be measured.

the complicated pattern of interaction among the fingers that formed in the two-layer experiments, a total of only 11 fingers from the two-layer experiments could be considered isolated and yielded flow rate, velocity, and cross-sectional area measurements. In addition, the flow rate through these fingers spanned only a very narrow range of $\mathbf{R}_f$ (0.03 to 0.09).

To obtain measurements that would give the behavior of d and v throughout the full range of $\mathbf{R}_f$ from 0 to 1, a second type of experiment was conducted where individual fingers were formed from 2 cm diameter tubes supplied by individual pumps. Each tube was covered by a fine wire mesh and applied directly to the top of the bottom layer constituting area sources of known strength. A comparable method was first used successfully by Saffman and Taylor (1958) in Hele-Shaw cells to study individual fingers and later by Glass *et al.* (1987) to study two-dimensional fingers in unsaturated porous media. Thus, the flow rate through the finger, Q_f, was supplied directly and $\mathbf{R}_f$ spanned the range from 0.18 to 0.94. Thirty-one fingers were simulated in the area source experiments, yielding in combination with the two-layer experiments a total of 42 individual fingers to evaluate the functions of $\mathbf{R}_f$ in Equations (3) and (5).

4. Results

The chamber-scale results of the two-layer experiments are presented in Table I. Figures 2a and 2b show chamber cross-sectional drawings of wet regions (shaded) with depth for experiments 1 and 3. Figure 2c shows a photograph of one of the 10 cm sections after it had been removed and some of the dry sand blown away. The fingers are seen to be fairly uniform, vertically standing cylinders. In a very homogeneous porous media, fingers meander only slightly in the horizontal and thus merger is less important than in more heterogeneous materials. However, we also find that many fingers form in a homogeneous media and as fingers become wider, interaction between fingers cannot be ignored. This is seen in the high flow rate experiment (experiment 3, Figure 2b) where many large fingers ran next to

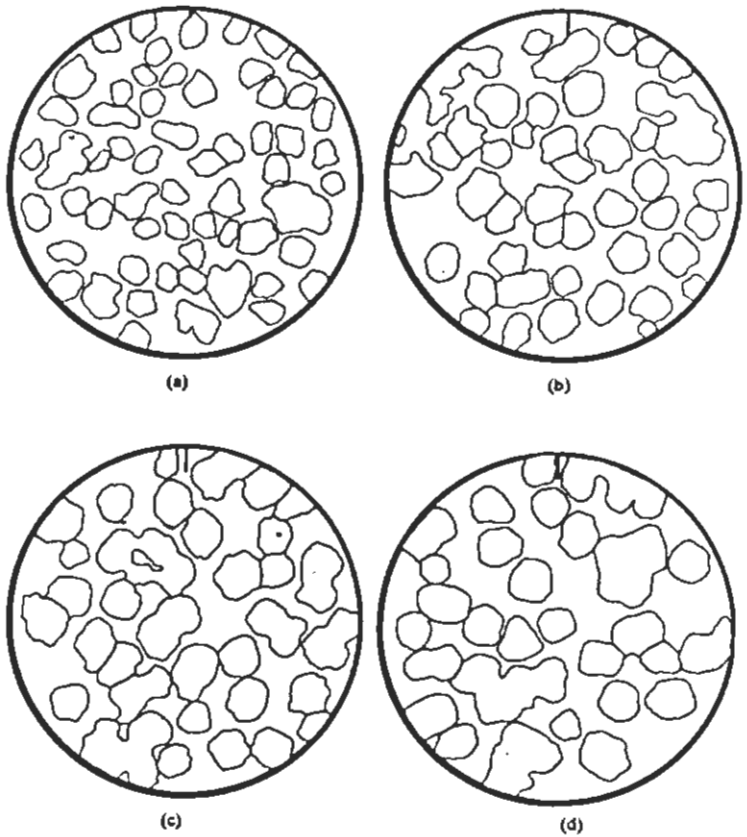

Fig. 2a. Chamber cross-sectional area drawings with depth showing fingers (shaded regions) for experiment 1. Depth from textural interface is: (a) 10 cm, (b) 20 cm, (c) 30 cm, and (d) 40 cm.

each other and it was impossible to find isolated fingers from which to obtain measurements.

Table I suggests, while not conclusively because of the small number of experiments performed, that an increase in flow rate through the system, and thus $\mathbf{R}_f$, increases the fraction of the chamber occupied by fingers and the average d and v of the fingers, but has little effect on the number of fingers that form. This same result was found earlier for two-dimensional systems (Glass *et al.*, 1989b).

On the scale of individual fingers we look for relationships between finger width, velocity, average moisture content, Q_f and $\mathbf{R}_f$. Figures 3, 4, and 5 show the effect

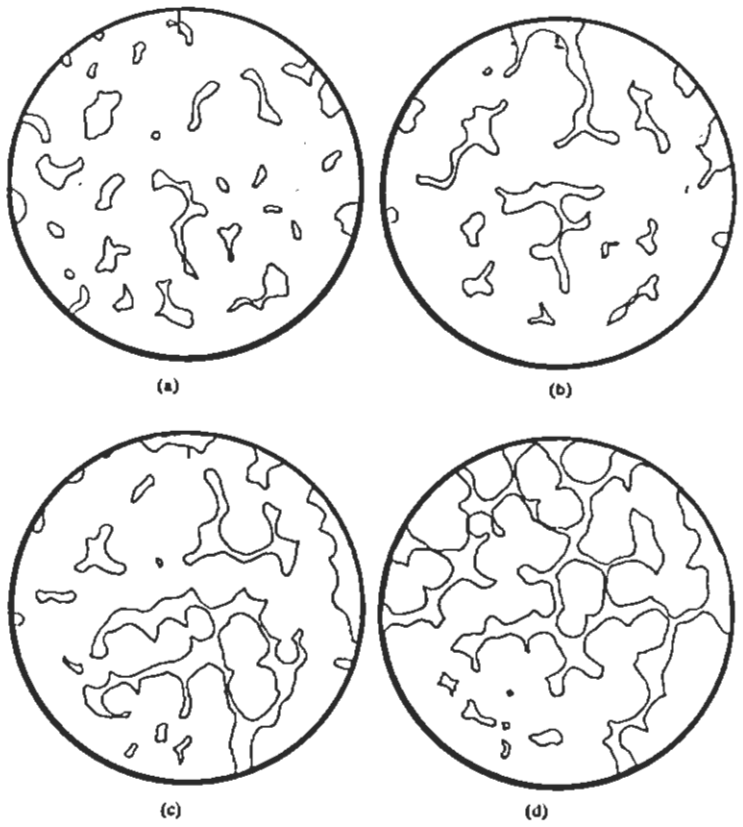

Fig. 2b. Chamber cross-sectional area drawings with depth showing fingers (shaded regions) for experiment 3. Depth from textural interface is: (a) 10 cm, (b) 20 cm, (c) 30 cm, and (d) 40 cm.

of Q_f on the finger velocity, average moisture content, and diameter, respectively. The average moisture content for a finger may be calculated by dividing the flow rate through the finger by the volume wetted per unit time calculated from the average velocity and cross-sectional area of a finger. The plots show that finger velocity, average moisture content, and diameter all are higher when Q_f is higher.

The slope of the finger velocity versus Q_f plot steadily decreases as Q_f increases and is expected to approach asymptotically the saturated pore velocity given by $K_s/(\theta_s - \theta_r)$, as was the case for two-dimensional fingers. The relationship between finger velocity and $\mathbf{R}_f$ is found to be a straight line throughout the full range of

Fig. 2c. Photograph of a 10 cm high section removed from the column after the dyed wet region was drawn (shown in Figures 2a,b). The photograph was taken from approximately the 8 o'clock position of Figure 2a,b.

$\mathbf{R}_F$ explored in the experiments with the least squares best fit line given by $v = 45.39\mathbf{R}_F + 11.4$ and an r^2 coefficient of 0.97. The velocity evaluated at $\mathbf{R}_F = 1$ gives the value v approached asymptotically in Figure 3 to be 56.8 cm/min. This value is near but 7% less than the value calculated from measured K_s (24.7 cm/min) and the porosity (calculated from the average bulk density to be 0.40) of 61.8 cm/min.

The average moisture content shown in Figure 4 increases rapidly at low Q_F, then levels off and, based on the results in two dimensions, should approach θ_s, which should be near the porosity, at high Q_F. However, the asymptote shown in Figure 4 of 0.30 is 25% lower than expected. In combination with the lower-than-expected maximum finger velocity shown in Figure 3, the results suggest that air entrapment may be removing pores from participation and thus playing a role in the phenomenon. With this in mind, we take the maximum moisture content of a finger from Figure 4 and denote it as $\alpha\theta_s$ with the corresponding maximum conductivity $\gamma K_s = K(\alpha\theta_s)$. These maximum values now replace θ_s and K_s in Equations (1) through (7) except where the ratio $S^2/K_s(\theta_s - \theta_i)$ occurs, as this combination is not very sensitive to the moisture content in the finger (Glass *et al.*, 1989a). The factors α and γ account for the effects of air entrainment and are included with θ_s and K_s, respectively, everywhere the flux through the finger or finger velocity is weighed against the maximum flux (γK_s) or velocity ($\gamma K_s/(\alpha\theta_s - \theta_i)$) under unit gradient, respectively (i.e. in the definitions of $\mathbf{R}_F$ and

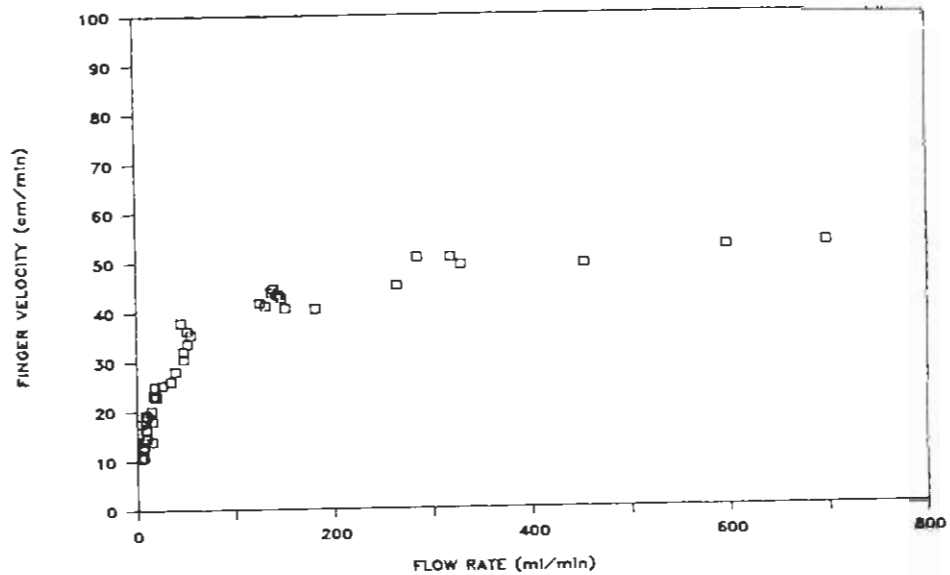

Fig. 3. Finger velocity, v, as a function of the flow rate through the finger, Q_F.

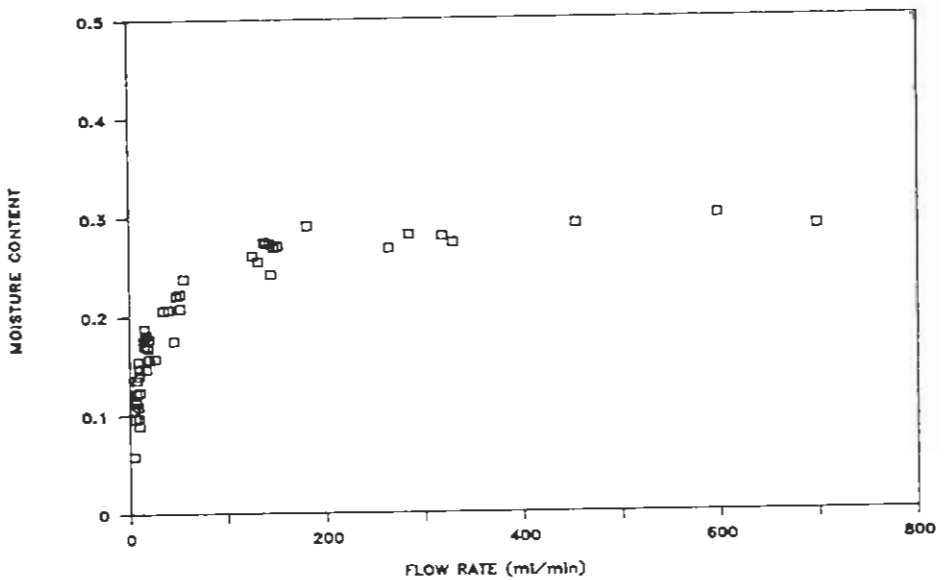

Fig. 4. Finger moisture content, θ_f, as a function of the flow rate through the finger, Q_F.

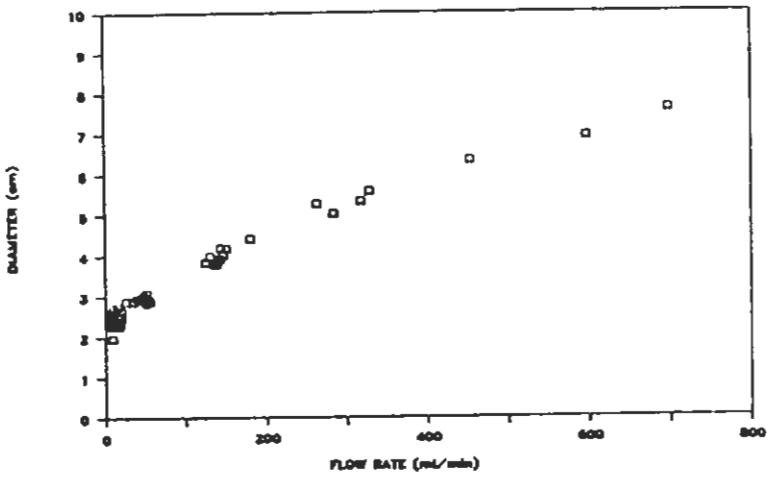

Fig. 5. Finger diameter, d, as a function of the flow rate through the finger, Q_f.

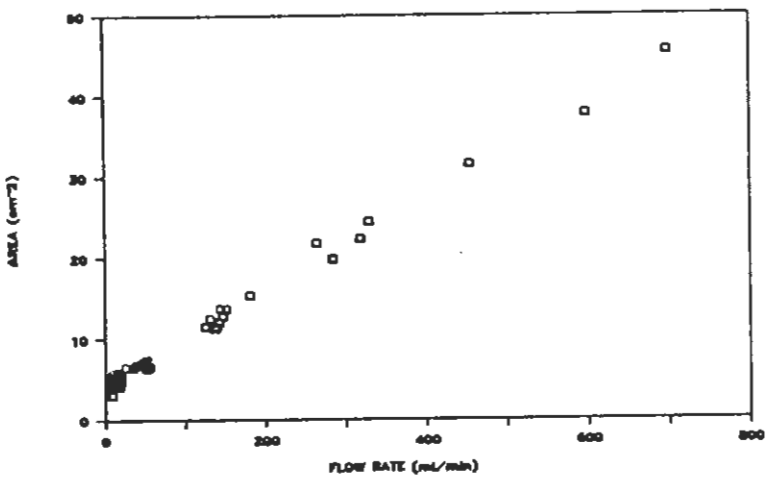

Fig. 6. Finger cross-sectional area, A, as a function of the flow rate through the finger, Q_f.

$\mathbf{R}_{vf}$). Thus N retains its former definition while $\mathbf{R}_f$ and $\mathbf{R}_{vf}$ will henceforth be redefined as $q_f/\gamma K_s$ and $\nu(\alpha\theta_r - \theta_i)/\gamma K_s$, respectively.

Figure 6 shows finger cross-sectional area to increase linearly with Q_f. This linear relation between finger cross-sectional area, A, and the flow through the finger, given by

$$A = m_1 Q_f + b_1 \tag{8}$$

may be used to find the form of $f_{df}(\mathbf{R}_f)$ in Equation (3). As Q_f becomes large, b_1 may be neglected and we find $1/m_1 = Q_f/A$. Because θ approaches $\alpha\theta_r$ and ν approaches $\gamma K_s/(\alpha\theta_r - \theta_i)$ for Q_f large, then Q_f/A must approach γK_s for Q_f large. Thus $m_1 = 1/\gamma K_s$ and

$$A = \frac{Q_f}{\gamma K_s} + b_1. \tag{9}$$

Writing Equation (9) in terms of the nondimensional finger flux-conductivity ratio $\mathbf{R}_f$, gives

$$A = \frac{b_1}{1 - \mathbf{R}_f}. \tag{10}$$

The finger cross-sectional area may be related to the finger diameter by $d = 2(A/\pi)^{1/2}$ so

$$d = \frac{2}{\pi^{1/2}}\left[\frac{b_1}{1 - \mathbf{R}_f}\right]^{1/2}. \tag{11}$$

Evaluating (11) and (3) for $\mathbf{R}_f$ at 0 yields b_1 as

$$b_1 = \frac{\pi}{4}\left[\frac{S^2}{(\theta_r - \theta_i)K_s} f_{df}(0)\right]^2, \tag{12}$$

where $f_{df}(0)$ is the value approached by f_{df} for $\mathbf{R}_f$ small. K_s was measured for the 14–20 sand using the constant head method to be 24.7 cm/min. The value of the square of the sorptivity evaluated between θ_i and θ_r at a potential of zero, S_0^2, was measured through a vertical infiltration experiment using an adaption of the method of Talsma (1969) proposed by Parlange *et al.* (1988). For this coarse sand, the method restricted experiments to small initial heads (5–10 cm) and short times (1–10 sec) thus increasing experimental error. The average S_0^2 value measured in six experiments was 64.8 cm²/min with a standard deviation of 16.5. The value of S with a supply pressure of ψ_{we} may be calculated using the approximate formula for S_0 of Parlange (1975),

$$S_0^2 = S^2 - 2K_s\psi_{we}(\theta_r - \theta_i) \tag{13}$$

ψ_{we} was estimated gravimetrically from a vertical rise experiment to be −3 cm. With θ_i taken to be zero and θ_r as 0.40, S^2 is calculated to be 5.5 cm²/min. A least

squares best fit line to the data in Figure 6 gives the slope, m_1, as 0.059 and the intercept, b_1, as 4.10 with an r^2 coefficient of 0.993. The value for γK_s obtained from the reciprocal of m_1 is 16.9 cm/min which yields a γ of 0.68. Taking θ_i as zero, $f_{dF}(0)$ is calculated from Equation (12) to be 4.1. Thus in the form of Equation (3),

$$d = 4.1 \frac{S^2}{K_s(\theta_s - \theta_i)} \left[\frac{1}{1 - \mathbf{R}_F}\right]^{1/2}. \tag{14}$$

A plot of observed d versus Equation (14) is shown in Figure 7. It should be noted that while b_1 is given precisely by Equation (8), the difficulties of measuring S^2 in coarse sands causes the value of $f_{dF}(0)$ in Equation (12) to be known much less precisely.

The product of finger cross-sectional area and velocity plotted versus the flow rate through a finger is seen in Figure 8 to also be a straight line. This linear relation given by

$$Av = m_2 Q_F + b_2 \tag{15}$$

may be used to obtain v in the form of Equation (4). As in Equation (8), when Q_F becomes large, b_2 may be neglected and $Q_F = Av/m_2$. For large Q_F the moisture content in the finger approaches $\alpha\theta_s$ so that $Q_F = Av(\alpha\theta_s - \theta_i)$ and thus $m_2 = 1/(\alpha\theta_s - \theta_i)$. Substitution for m_2 and rearrangement gives

$$v = \frac{q_F}{(\alpha\theta_s - \theta_i)} + \frac{b_2}{A}. \tag{16}$$

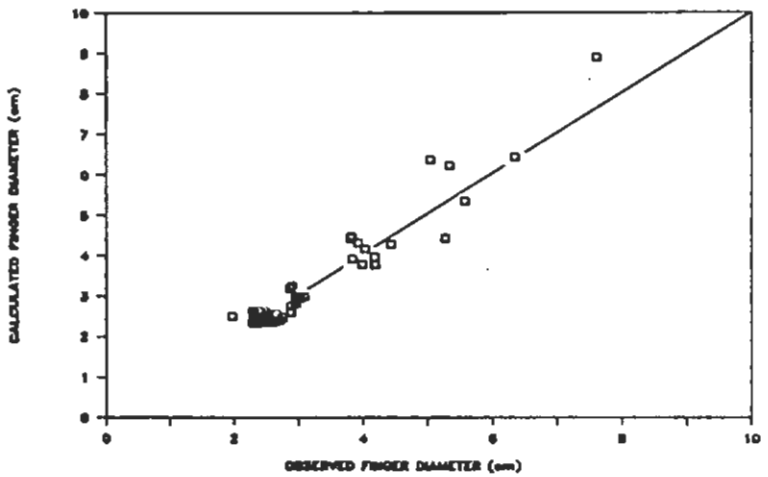

Fig. 7. Observed finger diameter, d, versus Equation (14). Line shows one-to-one correspondence.

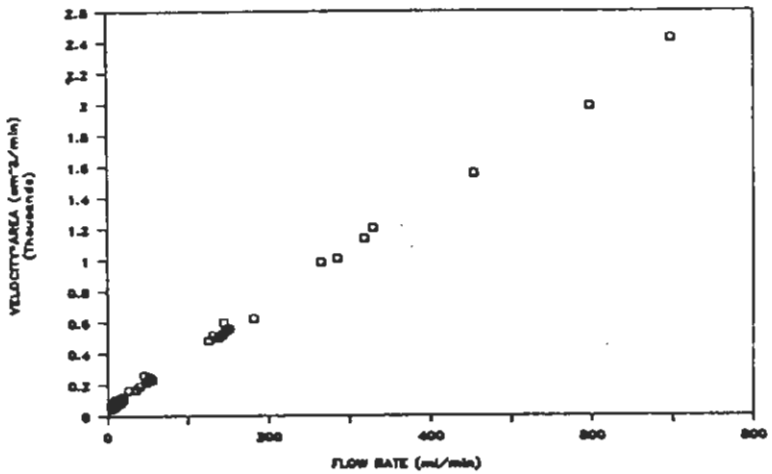

Fig. 8. Finger cross-sectional area * velocity, Av, as a function of flow rate through the finger, Q_F.

Substitution of Equation (10) for A yields

$$v = \frac{q_F}{(\alpha\theta_s - \theta_i)} + \frac{b_2}{b_1}[1 - \mathbf{R}_F] \tag{17}$$

Written in the form of Equation (5),

$$v = \frac{\gamma K_s}{(\alpha\theta_s - \theta_i)}\left[\frac{b_2(\alpha\theta_s - \theta_i)}{b_1\gamma K_s} + \mathbf{R}_F\left(1 - \frac{b_2(\alpha\theta_s - \theta_i)}{b_1\gamma K_s}\right)\right] \tag{18}$$

While it is clear that finger velocity will be zero when $\mathbf{R}_F = 0$, our data suggest that for $\mathbf{R}_F$ small but positive v approaches a limit v_{min} which is nonzero. The constant b_2 should be a product of the minimum finger area given by b_1 and v_{min} given by

$$v_{min} = \frac{C_2\gamma K_s}{(\alpha\theta_s - \theta_i)}, \tag{19}$$

where C_2 is simply a factor that reduces the maximum velocity to v_{min}. Thus

$$b_2 = b_1 C_2 \frac{\gamma K_2}{(\alpha\theta_s - \theta_i)} \tag{20}$$

and substitution into (18) yields

$$v = \frac{\gamma K_s}{(\alpha\theta_s - \theta_i)}[C_2 + \mathbf{R}_F(1 - C_2)]. \tag{21}$$

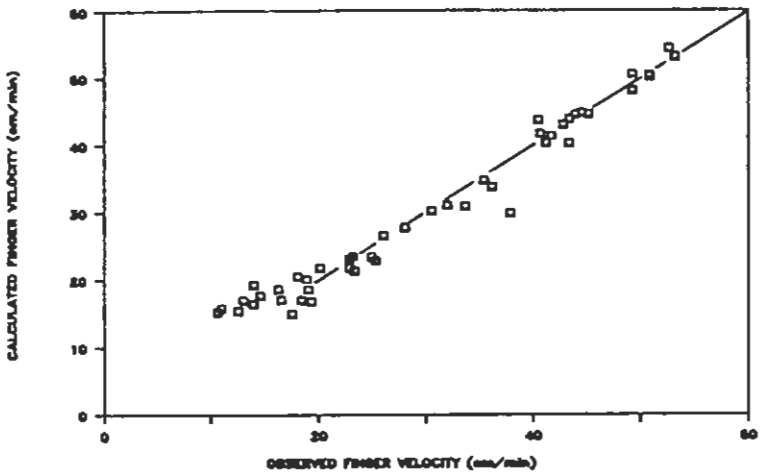

Fig. 9. Observed finger velocity, v, versus Equation (21). Line shows one-to-one correspondence.

A least squares, best-fit line to the data in Figure 8 gives m_2 as 3.36 and b_2 as 52.23 with an r^2 of 0.998. Thus, with $\alpha\theta_r$ as 0.30 and with the values of K_s and b_1 given above, C_2 is calculated to be 0.23. A plot of observed v versus Equation (21) is shown in Figure 9.

5. Discussion

The maximum moisture content, maximum finger velocity, and maximum flux through the finger as given by the reciprocal slope of the line in Figure 6 are all less than the values expected from the results of the two-dimensional experiments, θ_s, $K_s/(\theta_s - \theta_i)$, and K_s, respectively (Glass *et al.*, 1989b). Error in the measurement of finger cross-sectional area (probably overestimation) and finger velocity (probably underestimation) for three-dimensional fingers is much greater than for two-dimensional fingers. While adjustment of the measured values in the proper direction does increase both α and γ, corrections to make them both 1 lead to nonphysical results (a θ_r of approximately 0.46). Thus, it is much more likely that three-dimensional fingers are affected by air entrapment while those in two-dimensional systems are not. The effect of air entrapment is easily accounted for in the equations for d and v (Equations (14) and (21), respectively) through the factors α and γ. It is not known whether α and γ could be measured independently or will have to be measured from fingering experiments. Much additional experimentation is required to resolve the effects of air entrapment; however, this is true for stable infiltration cases as well.

Through experimentation in unstable two-dimensional flow fields as caused by a finer layer overlaying a coarser layer, Glass *et al.* (1989b) evaluated the functions $f_{d2}(\mathbf{R}_F)$ and $f_{v2}(\mathbf{R}_F)$ for two-dimensional fingers yielding

$$d_{2d} = C_{12d} \frac{S^2}{K_s(\theta_s - \theta_i)} \left[\frac{1}{1 - \mathbf{R}_F}\right] \tag{22}$$

and

$$v_{2d} = \frac{K_s}{(\theta_s - \theta_i)} [C_{22d} + \mathbf{R}_F(1 - C_{22d})], \tag{23}$$

where C_{12d} was found to be 3 and C_{22d} to be 0.1 and the subscript 2d denotes two-dimensional.

The functional form of the dependence of finger width and diameter on $\mathbf{R}_F$ in two and three dimensions is seen to be different by a power of one-half as finger width goes as $(1 - \mathbf{R}_F)^{-1}$ (Equation (22)) while finger diameter goes as $(1 - \mathbf{R}_F)^{-1/2}$ (Equation (14)). However, because in two-dimensional systems, all definitions are per unit thickness and not per unit area, finger width may be considered an area per unit thickness and so in comparison with Equation (10), the cross-sectional area per unit thickness in two dimensions and the cross-sectional area in three dimensions have the same behavior in $\mathbf{R}_F$.

The behavior of finger velocity with $\mathbf{R}_F$ in two- and three-dimensional systems is seen to have exactly the same form when written with respect to the maximum and minimum finger velocity. C_2 and C_{22d} are simply the ratio of the minimum finger velocity to the maximum finger velocity. This ratio and the maximum velocity are different for two- and three-dimensional fingers with air entrapment again playing a role.

With d given by Equation (14), Equation (6) may be written to yield the stability condition

$$L_s < d. \tag{24}$$

As discussed earlier, to apply Equation (24) easily, a relation is needed for β as defined in Equation (7) so that Equation (14), now written for $\bar{d}$, may be written in terms of q_S. In two-dimensional homogeneous systems β is found experimentally to be

$$\beta = 1/\overline{\mathbf{R}_F}, \tag{25}$$

where $\overline{\mathbf{R}_F}$ is defined with $\overline{q_F}$. While the two-layer data for the current experiments are too limited to allow an independent determination of a relation for β, a value of β calculated from Equation (25) for experiments 2 and 4 show Equation (25) to be a factor of 3 to 4 too high. Equation (25), however, was found for the two-dimensional case to overestimate β for very small $\overline{\mathbf{R}_F}$ as it was in experiments 2 and 4 (0.05 and 0.06, respectively). It is clear that additional experimentation with full unstable flow fields is required to resolve the formulation for β.

The linear stability analysis of Parlange and Hill (1976) yielded a relation for the expected two-dimensional finger width that is near to the behavior found experimentally in Equation (22). Guided by experimental results, Glass *et al.* (1989b) reinterpreted the analysis of Parlange and Hill and incorporated the experimentally determined relation for β (Equation (25)) to obtain Equation (22) with C_1 as π, thus showing close correspondence between linear stability theory and experiment for two-dimensional fingers in isotropic, homogeneous, porous media. Similar analysis applied to three-dimensional fingers to determine the constant in Equation (14) requires proper representation of finger geometry and will be presented in a subsequent paper.

While Equations (14) and (21) describe well the dependence of d and v on $\mathbb{R}_F$, respectively, the scaling factors for each given by $S^2/[(\alpha\theta_s - \theta_i)\gamma K_s]$ and $\gamma K_s/(\alpha\theta_s - \theta_i)$ must be verified. This may be accomplished by systematically varying the properties of the bottom layer. Three-dimensional studies such as this one are extremely labor intensive compared to two-dimensional studies. Because we now have the relationship between two- and three-dimensional formulations for d and v as functions of $\mathbb{R}_F$, scaling verification may be most efficiently accomplished through two-dimensional experimentation.

6. Conclusion

For ponded infiltration into initially dry, two-layer sand systems where a fine-textured top layer overlays a coarse bottom layer, wetting front instability is observed if the diameter of the system is greater than the diameter of the fingers that will form in the bottom layer. Through direct simulation of individual fingers in a coarse bottom layer, the dependence of finger moisture content, cross-sectional area, diameter, and velocity on the flux through a finger and the dimensionless flux-conductivity ratio, $\mathbb{R}_F$, is determined. A decrease in the maximum moisture content and velocity approached by three-dimensional fingers over that approached by two-dimensional fingers suggests air entrapment to be much more significant in the former than in the latter. $\mathbb{R}_F$ as defined by the ratio of the flux through a finger to the maximum flux under unit gradient is easily adjusted for air entrapment effects. Finger cross-sectional area is found to be proportional to $(1 - \mathbb{R}_F)^{-1}$ in three dimensions, while in two dimensions, finger cross-sectional area per unit thickness (finger width) is proportional to $(1 - \mathbb{R}_F)^{-1}$. Finger velocity for both two- and three-dimensional fingers is found to have the same dependence on $\mathbb{R}_F$ when written in terms of the maximum and minimum finger velocities.

Acknowledgement

This research was supported in part by EPA grant R-812919-01-1: 'Wetting front instability in layered soils and its inclusion in monitoring and modeling techniques' and the U.S. Department of Energy (DOE), Office of Civilian Radioactive Waste Management, Yucca Mountain Project, contract DE-AC04-76DP00789.

References

Chouke, R. L., Van Meurs, P., and Van der Poel, C., 1959, The instability of slow immiscible, viscous liquid-liquid displacements in porous media, *Trans. Am. Inst. Min. Eng.* **216**: T.P.8073.

Diment, G. A. and Watson, K. K., 1985, Stability analysis of water movement in unsaturated porous materials. 3. Experimental Studies, *Water Resour. Res.* **21**, 979-984.

Glass, R. J., Parlange, J.-Y., and Steenhuis, T. S., 1987, Water infiltration in layered soils where a fine textured layer overlays a coarse sand, *Proc. Internat. Conf. Infiltration Development and Application*, Hawaii, 5-9 Jan. 1987, 66-81.

Glass, R. J., Parlange, J.-Y., and Steenhuis, T. S., 1989a, Wetting front instability I: Theoretical discussion and dimensional analysis, *Water Resour. Res.* **24**, 1187-1194.

Glass, R. J. and Steenhuis, T. S., 1984, Factors influencing infiltration flow instability and movement of toxics in layered sandy soils, ASAE Technical Paper No. 84-2508.

Glass, R. J., Steenhuis, T. S., and Parlange, J.-Y., 1988, Wetting front instability as a rapid and far-reaching hydrologic process in the vadose zone, *J. Contaminant Hydrology* **3**, 207-226.

Glass, R. J., Steenhuis, T. S., and Parlange, J.-Y., 1989b, Wetting front instability II: Experimental determination of relationships between system parameters and two-dimensional unstable flow field behavior in initially dry porous media, *Water Resour. Res.* **24**, 1195-1207.

Glass, R. J., Steenhuis, T. S., and Parlange, J.-Y., 1989c, Mechanism for finger persistence in homogeneous unsaturated porous media: Theory and verification, *Soil Sci.* **148**, 60-70.

Green, T., 1984, Scales for double-diffusive fingering in porous media, *Water Resour. Res.* **20**, 1225-1229.

Haverkamp, R. and Parlange, J.-Y., 1986, Predicting the water-retention curve from particle-size distribution: 1. Sandy soils without organic matter, *Soil Sci.* **142**, 325-339.

Hendrickx, J. M. H., Dekker, L. W., Van Zuilen, E. J., and Boersma, O. H., 1988, Water and solute movement through a water repellent sand soil with grasscover, Presented at the International Conference and Workshop on Validation of Flow and Transport Models for the Unsaturated Zone, Ruidoso, New Mexico, 23-26, May 1988.

Hill, D. E. and Parlange, J.-Y., 1972, Wetting front instability in layered soils, *Soil Sci. Soc. Am. Proc.* **36**, 697-702.

Homsy, G. M., 1987, Viscous fingering in porous media, *Ann. Rev. Fluid Mech.* **19**, 271-311.

Miller, D. E. and Gardner, W. H., 1962, Water infiltration into stratified soil, *Soil Sci. Soc. Amer. Proc.* **26**, 115-119.

Miller, E. E. and Miller, R. D., 1956, Physical theory for capillary flow phenomena, *J. Appl. Phys.* **27**, 324-332.

Parlange, J.-Y., 1975, On solving the flow equation in unsaturated soils by optimization. Horizontal infiltration, *Soil Sci. Soc. Am. Proc.* **39**, 415-418.

Parlange, J.-Y. and Hill, D. E., 1976, Theoretical analysis of wetting front instability in soils, *Soil Sci.* **122**, 236-239.

Parlange, J.-Y., Haverkamp, R., Rose, C. W., and Phillips, I., 1988, Sorptivity and conductivity measurement, *Soil Sci.* **145**, 385-388.

Peck, A. J., 1965, Moisture profile development and air compression during water uptake by bounded porous bodies: 3 vertical columns, *Soil Sci.* **100**, 44-51.

Philip, J. R., 1975, Stability analysis of infiltration, *Soil Sci. Soc. Am. Proc.* **39**, 1042-1049.

Saffman, P. G. and Taylor, G., 1958, The penetration of a fluid into a porous medium or Hele-Shaw cell containing a more viscous liquid, *Proc. Roy. Soc. London.* **A245**, 312-331.

Smith, W. O., 1967, Infiltration in sand and its relation to ground water recharge, *Water Resour. Res.* **3**, 539-555.

Starr, J. L., DeRoo, H. C., Frink, C. R., and Parlange, J.-Y., 1978, Leaching characteristics of a layered field soil, *Soil Sci. Soc. Am. J.* **42**, 376-391.

Starr, J. L., Parlange, J.-Y., and Frink, C. R., 1986, Water and chloride movement through a layered field soil, *Soil Sci. Soc. Am. J.* **50**, 1384–1390.

Tabuchi, T., 1961, Infiltration and ensuing percolation in columns of layered glass particles packed in laboratory, *Nogyo dobuku kenkyn, Bessatsu* (*Trans. Agr. Eng. Soc., Japan*) **1**, 13–19.

Talsma, T., 1969, In situ measurement of sorptivity, *Aust. J. Soil Res.* **7**, 269–276.

Tamai, N., Asaeda, T., and Jeevaraj, C. G., 1987, Fingering in two-dimensional, homogeneous, unsaturated porous media, *Soil Sci.* **144**, 107–112.

Turner, J. S., 1985, Multicomponent Convection, *Ann. Rev. Fluid Mech.* **17**, 11–44.

Van Ommen, H. C. and Dijksma, R., 1988, Analysis of transport in a coupled unsaturated-saturated system, Presented at the International Conference and Workshop on Validation of Flow and Transport Models for the Unsaturated Zone, Ruidoso, New Mexico. 23–26 May 1988.

Van Ommen, H. C., Dekker, L. W., Dijksma, R., Hulshof, J., and Van der Molen, W. H., 1988, A new technique for evaluating the presence of preferential flow paths in non-structured soils, *Soil Sci. Soc. Am. J.* **55**, 1192–1193.

White, I., Colombera, P. M., and Philip, J. R., 1976, Experimental study of wetting front instability induced by sudden change of pressure gradient, *Soil Sci. Soc. Am. J.* **40**, 824–829.